International Association of Scientific Innovation and Research (IASIR)
(An Association Unifying the Sciences, Engineering, and Applied Research)

ISSN (Print): 2279-0047
ISSN (Online): 2279-0055

International Journal of Emerging Technologies in Computational and Applied Sciences (IJETCAS)

www.iasir.net

Design and Analysis of Solar Power Switched Inductor and Switched Capacitor for DC Distribution System

Mr. D.Saravanakumar[1], Mrs. G.Gaayathri[2]
[1]Assistant Professor, Electrical and Electronics Engineering, Nehru Institute of Engineering and Technology, Coimbatore, Tamil Nadu, INDIA
[2]Assistant Professor, Computer Science Engineering, Hindusthan College of Engineering and Technology, Coimbatore, Tamil Nadu, INDIA

Abstract*: This paper proposes a high step-up solar power optimizer (SPO) that efficiently harvests maximum energy from a photovoltaic (PV) panel then outputs energy to a dc-microgrid. Its structure switched inductor and switched capacitor technologies to realize high step-up voltage gain. The leakage inductance energy of the coupled inductor can be recycled to re- duce voltage stress and power losses. A low voltage rating and low-conduction resistance switch improves system efficiency by employing the incremental conductance method for the maximum power point tracking (MPPT) algorithm. Because of its high tracking accuracy, the method is widely used in the energy harvesting of PV systems. laboratory prototypes of the proposed SPO that have an input voltage range of 40 to 60V and a maximum PV output power of 400 V/300 W are applied.*

Index Terms: High step-up voltage gain, maximum power point tracking (MPPT), solar power optimizer (SPO).

I. INTRODUCTION

Fossil fuels continue to be depleted, and their use has been instrument to climate change, a problem that grows more severe. The proposed converter has the following features: 1) its voltage conversion ratio is efficiently increased by using the switched capacitor and coupled inductor techniques; 2) the leak- age inductance energy of the coupled inductor can be recycled to increase efficiency, and the voltage spike on the active switch is restrained; 3) the floating active switch isolates the PV panel's energy during nonoperating conditions, thereby preventing any potential electric hazard to humans or facilities. The MPPT control algorithm exhibits high-tracking efficiency; hence, it is widely used in the energy harvesting of PV systems.

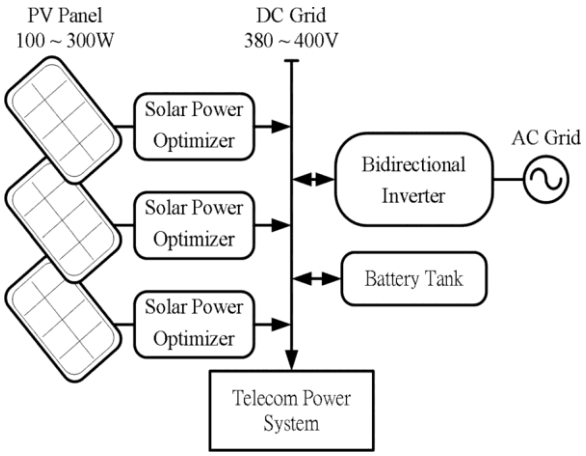

Fig. 1: Configuration of multiple parallel SPO for a dc-microgrid system.

The system energy's harvesting efficiency and entails high costs. A solar power optimizer (SPO) was developed as an alternative to maximize energy harvest from each individual PV module. An SPO is used as a dc–dc converter with maximum power point tracking (MPPT), which increases PV panel voltage to optimum voltage levels for a dc microgrid connection or through a dc–ac inverter for electricity [3]–[6]. Fig. 1 shows a single PV panel's energy, which passes through an SPO to a dc micro- grid system. A 400 V dc-microgrid system was proposed as an energy-efficient distribution option for data center systems and telecommunication facilities [7]. The SPO attempts to improve the use of distributed renewable resources and lower system cost. It may also potentially improve the efficiency of PV systems, has an anti shadow effect, and can monitor the status of PV modules [8]. Moreover, the dc-grid voltage is regulated by bidirectional inverter and battery tank.

In case of low-loading condition, the redundant energy will store into battery or through bidirectional inverter to ac grid.

The maximum power point (MPP) voltage range of a single PV panel ranges from 15 to 40 V and has a power capacity of about 100 to 300 W [9]. An SPO has a high step-up converter that increases low-input voltage to a sufficient volt- age level. Various step-up dc–dc converter topologies include a conventional boost and flyback converters [10], [11], switched- inductor converter, and switched capacitor converter [12]–[16], as well as a transformerless switched capacitor types [17], [18], voltage-lift types [19]–[21], capacitor–diode voltage multipliers [22]–[25], and boost types that are integrated with coupled inductors [26]–[29]. With increasing voltage gain, recycling the leakage inductance energy of a coupled inductor will reduce the voltage stress on the active switch, which enables the coupled inductor and voltage multiplier or voltage-lift technique to realize high-voltage gain [9]–[29].

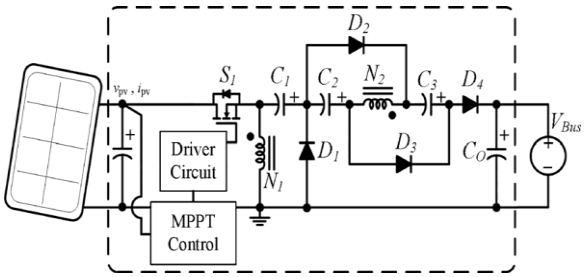

Fig. 2: Configuration of the proposed SPO.

The proposed SPO is shown in Fig. 2; its configuration is based on a high step-up dc–dc converter with an MPPT con- trol circuit. The converter includes a floating active switch S and a coupled inductor T_1 with primary winding N_1 , which is similar to the input inductor of a conventional boost converter capacitor C_1 , and diode D_1 recycle leakage inductance energy from N_1 . Secondary winding N_2 is connected to another pair of capacitors, C_2 and C_3, and to diodes D_2 and D_3. Rectifier diode D_4 connects to output capacitor C_o and load R. The duty ratio is modulated by the MPPT algorithm, which uses the incre- mental conductance method [30]–[35] that is employed in the proposed SPO. It detects PV module voltage V_{pv} and current I_{pv} to determine the increase and decrease in the duty cycle of the dc converter. Therefore, the MPP can be obtained by compar- ing instantaneous conductance I/V and incremental conductance dI/dV. The algorithm is programmed into TMS320LF2407A, a digital signal microprocessor.

The proposed converter has the following features: 1) its voltage conversion ratio is efficiently increased by using the switched capacitor and coupled inductor techniques; 2) the leak- age inductance energy of the coupled inductor can be recycled to increase efficiency, and the voltage spike on the active switch is restrained; 3) the floating active switch isolates the PV panel's energy during nonoperating conditions, thereby preventing any potential electric hazard to humans or facilities. The MPPT control algorithm exhibits high-tracking efficiency; hence, it is widely used in the energy harvesting of PV systems.

The rest of the paper is organized as follows. Sections II and III discuss the operating principle and steady-state analysis of the proposed converter, respectively. Section IV addresses the practical implementation and component selection of the proposed converter. Section V presents the experimental results, and VI concludes the paper.

II. OPERATING PRINCIPLES

The operating principles for continuous conduction mode (CCM) and discontinuous conduction mode (DCM) are presented in detail. Fig. 3 illustrates a typical waveform of several major components in CCM operation during one switching period.

To simplify the circuit analysis of the proposed converter, the following assumptions are made:

1) All components are ideal, except for the leakage inductance of coupled inductor $T1$, which is taken into account. On-state resistance RDS (ON) and all the parasitic capacitances of main switch S are disregarded, as are the forward voltage drops of diodes $D1$ to $D4$;

2) Capacitors $C1$ to $C3$ and Co are sufficiently large that the voltages across them are considered constant;

3) The equivalent series resistance (ESR) of capacitors $C1$ to $C3$ and Co , as well as the parasitic resistance of coupled inductor $T1$ is Neglected;

4) Turns ratio n of coupled inductor $T1$ windings is equal to $N2$ /$N1$.

The CCM operating modes are described as follows.

A. CCM Operation

Mode I [t0, t1]: During this interval, switch S and diodes $D2$ and $D3$ are conducted; diodes $D1$ and $D4$ are turned OFF. The current flow path is shown in Fig. 4(a). Magnetizing inductor Lm continues to release energy to capacitors $C2$ and $C3$ through secondary winding$N2$ of coupled inductor $T1$. Leakage inductance Lk 1

denotes the stored energy from source energy *V*in . The energy that is stored in capacitor *Co* is constantly discharged to load *R*. This mode ends when increasing *iLk*1 is equal to decreasing i_{Lm} at $t = t_1$

$$vLm = Vin \quad (1)$$

$$\Delta iLm = Vin/Lm(t_1-t_0) \quad (2)$$

*Mode II [t*1 , *t*2 *]:* During this interval, switch *S* and diode *D*4 are conducted. Source energy *V*in is serially connected to *C*1, *C*2 , and *C*3 , and secondary winding *N*2 ; *Lk*2 discharges the energy that is stored in charge output capacitor *Co* and loads *R*. Meanwhile, magnetizing inductor *Lm* also receives energy from *V*in. The current flow path is shown in Fig. 4(b). This mode ends when switch S is turned OFF at $t = t2$

$$vLm = \frac{Vo - Vin - Vc1 - Vc2 - Vc3}{n} \quad (3)$$

$$n = \frac{N_2}{N_1} \quad (4)$$

$$\Delta i_{Lm} = \frac{V_o - V_{in} - V_{c1} - V_{c2} - V_{c3} \cdot (t_2 - t_1)}{n \cdot L_m} \quad (5)$$

*Mode III [t*2 , *t*3 *]:* During this transition interval, switch *S* and diodes *D*2 and *D*3 are turned OFF, and diodes *D*1 and *D*4 are conducted. The current flow path is shown in Fig. 4(c). The energy stored in leakage inductance *Lk* 1 instantly flows through the diode *D*1 to charge capacitor *C*1 . The energy is released to magnetizing inductor *Lm* through coupled inductor *T*1 , which is serially connected to *C*1, *C*2 , and *C*3 , and secondary winding *N*2 ; *Lk*2 discharges the energy that is stored in charge output capacitor *Co* and loads *R*. This mode ends when decreasing i_{Lk1} is equal to increasing i_{Lm} at $t = t_3$

$$vLm = -Vc1 \quad (6)$$

*Mode IV [t*3 , *t*4 *]:* During this interval, switch *S* and diode *D*4 are turned OFF, and diodes *D*1,*D*2 , and *D*3 are conducted.

The current flow path is shown in Fig. 4(d). Leakage inductance *Lk* 1 continues to release energy to charge capacitor *C*1 through diode *D*1 . Magnetizing inductor *Lm* through coupled inductor *T*1 transfers energy to capacitors *C*2 and *C*3 . The energy that is stored in capacitor *Co* is constantly discharged to load *R*. This mode ends when decreasing i_{Lk1} is zero at $t = t_4$

$$v_{Lm} = -V_{c1} \quad (7)$$

*Mode V [t*4 , *t*5 *]:* During this interval, diodes *D*2 and *D*3 are conducted. The current flow path is shown in Fig. 4(e). Magnetizing inductor *Lm* constantly transfers energy to secondary winding *N*2 , and charges capacitors *C*2 and *C*3 . The energy that is stored in capacitor *Co* is constantly discharged to load *R*. This mode ends when switch S is turned ON at the beginning of the next switching period

$$vLm = -\frac{Vc2}{n} = -\frac{Vc3}{n} \quad (8)$$

B. DCM Operation

Fig. 5 illustrates a typical waveform of several major components in DCM operation during one switching period.

Mode I [t0, t1]: During this interval, switch S and D4 are conducted, and diodes D1,D2 , and D3 are turned OFF. The current flowpath is shown in Fig. 6(a).Magnetizing inductorLm with leakage inductance Lk 1 stores energy from source energy Vin . Meanwhile, source energy Vin is also serially connected to capacitors C1, C2 , and C3 , and secondary winding N2 to charge capacitor Co and load R. This mode ends when switch S is turned OFF at t = t1

$$vLm = Vin = \frac{Vo - Vin - Vc1 - Vc2 - Vc3}{n} \quad (9)$$

Mode II [t1, t2]: During this transition interval, switch S and diodes D2 and D3 are turned OFF, and diodes D1 and D4 are conducted. The current flow path is shown in Fig. 6(b). The energy stored in leakage inductance Lk 1 instantly flows through the diodeD1 to charge capacitor C1 ; this energy is also released to magnetizing inductor Lm through the coupled inductor T1 series that is connected to C1, C2 , and C3 , secondary winding N2 , and Lk2 to charge output capacitor Co and load R. This mode ends when decreasing iD4 is zero at t = t2

$$\frac{\Delta i_{Lm} = V_{in} \cdot (t_1 - t_0)}{L_m} = \frac{V_o - V_{in} - V_{c1} - V_{c2} - Vc3}{n \cdot L_m} \quad (10)$$

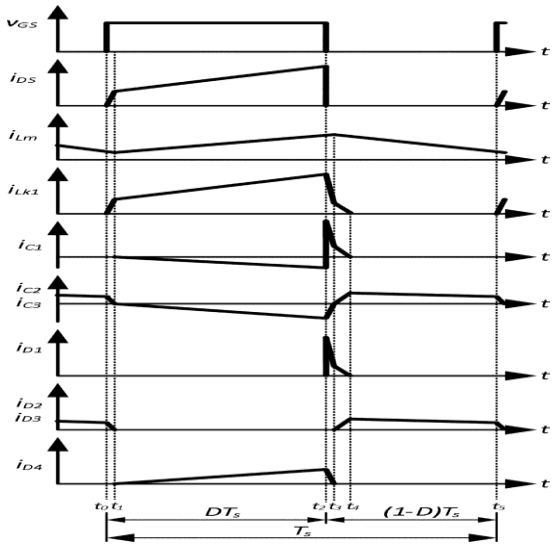

Fig. 3. Typical waveforms of the proposed converter in CCM operation.

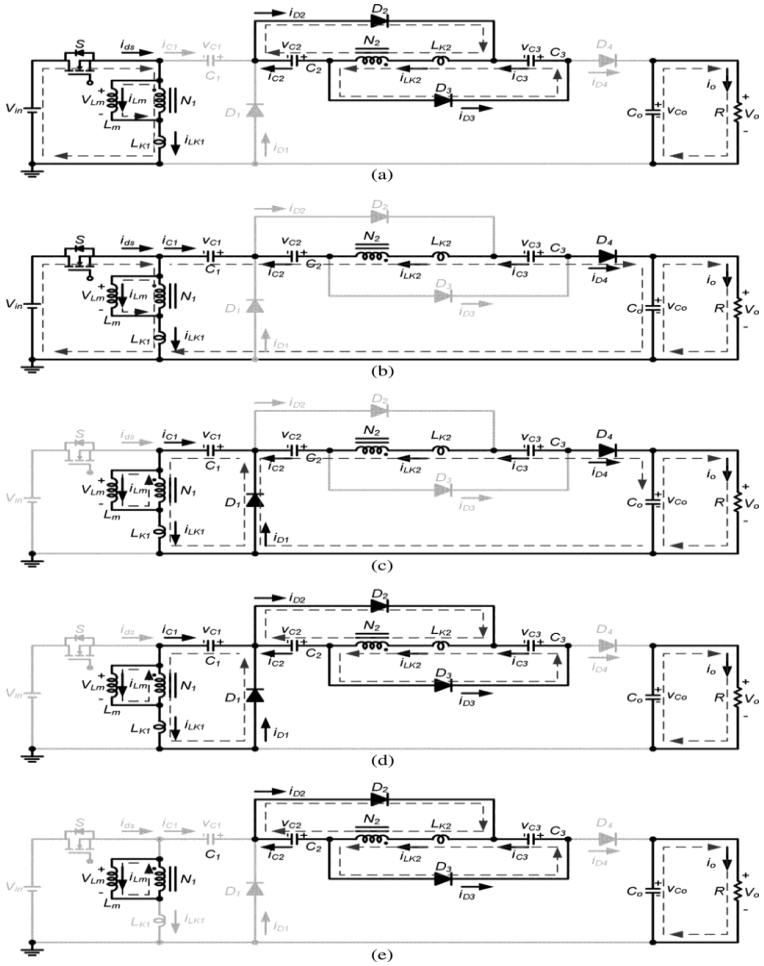

Fig. 4. Current flow path in five operating modes during one switching period in DCM operation: (a) Mode I, (b) Mode II, (c) Mode III, (d) Mode IV, and (e) Mode V.

Mode III [t2, t3]: During this transition interval, switch S and diode D4 are turned OFF, and diodes D1,D2 , and D3 are conducted. The current flow path is shown in Fig. 6(c). Leakage inductance Lk 1 continues to release energy to charge capacitor C1 through diode D1 . Magnetizing inductor Lm transfers energy to capacitors C2 and C3 through coupled inductor T1. The energy stored in capacitor Co is constantly discharged to load R.

Mode IV [t3, t4]: During this interval, switch S, diodes D1 and D4 are turned OFF, and diodes D2 and D3 are conducted. The current flow path is shown in Fig. 6(d).Magnetizing inductor Lm constantly transfers

energy to secondary winding N2 and charges capacitors C2 and C3. The energy that is stored in capacitor Co is constantly discharged to load R. This mode ends when decreasing iLm is zero at t = t4.

Mode V [t4, t5]: During this interval, the switch and all the diodes are turned OFF. The current flow path is shown in Fig. 6(e). The energy that is stored in capacitor *Co* is constantly discharged to load *R*. This mode ends when switch S is turned ON at the beginning of the next switching period

III. STEADY-STATE ANALYSIS

A. CCM Operation

Only steady-state analysis is considered during CCM operation,and the leakage inductances at primary and secondary sides are disregarded. Applying a volt-second balance on the magnetizing inductance L_m yields

$$\int_0^{DT_S} V_{\text{in}}\,dt + \int_{DT_S}^{T_S} (-V_{C1})\,dt = 0$$

$$\int_0^{DT_S} (nV_{\text{in}})\,dt + \int_{DT_S}^{T_S} (-V_{C2})\,dt = 0$$

B. BCM Operating Conditions

The leakage inductances at primary and secondary sides are disregarded in this approach. Applying volt-second balance on magnetizing inductance Lm, deriving

$$\int_0^{DT_S} V_{\text{in}}\,dt + \int_{DT_S}^{D_L T_S} (-V_{C1})\,dt = 0$$

IV. DESIGN CONSIDERATIONS OF THE PROPOSED CONVERTER

A 300 W SPO prototype is presented to verify the feasibility of the proposed converter. The considerations for component parameter design and selection are described as follows.

A. Duty Ratio and Turns Ratio

The largest voltage gain is 20 (see Table I). The turns ratio can be set to 2–6 [see (28) and Fig. 7]. When n = 2, the duty ratio is equal to 77.2%. When the duty ratio is larger than 70%, conduction losses significantly increase. If turn ratio n ≥ 5 results in a small duty ratio and low magnetizing inductance, but a high peak current over the active switch occurs. Therefore, n = 4 is the appropriate choice. As determined with (28), duty ratio D is 62.5%.

B. Magnetizing Inductor

Substituting the values of duty ratio, turns ratio, and operating frequency into (43) yields a boundary magnetizing inductance of 20.86 μH. This value can also be obtained by using Fig. 10. However, the actual magnetizing inductance is 21.87 μH and the leakage inductance is about 0.22 μH.

C. Active Switch and Diodes

The highest input voltage is 40 V and its corresponding duty ratio is 35.7%. The voltage stress of diodes D1 to D4 can be obtained by

$$V_{D1} = \frac{1}{1-D} \cdot V_{\text{in}} = \frac{1}{1-0.357} \cdot 40 = 62.2\,\text{V}$$

By considering the parasitic capacitor and inductor effects on the actual components and the PCB, the voltage rating of MOSFETs is higher than the calculated value. The nominal voltage of IXFX150N15 drain-source is 150V, which is denoted as *S*. Diode D_1 uses MBR30100CT, which has a voltage ratingof 100 V. Diodes D_2 and D_3 are UF3003. The voltage rating is 300 V and BYR29-600 is a 600 V diode denoted as D_4 .

D. Switched Capacitors

The voltage ripple is set to 2% of the capacitor voltage. The voltage across capacitors C1 to Co can be obtained by

$$C_1 = \frac{I_o T_S}{\Delta V_{C1}} = \frac{0.75 \cdot 20 \times 10^{-6}}{0.02 \cdot \frac{0.625}{1-0.625} \cdot 20} = 22.5\,\mu\text{F}$$

$$C_2 = C_3 = \frac{I_o T_S}{\Delta V_{C2}} = \frac{4.5 \times 10^{-6}}{4} \cong 5.6\,\mu\text{F}$$

$$C_o = \frac{I_o D T_S}{\Delta V_o} = \frac{0.75 \cdot 0.625 \cdot 20 \cdot 10^{-6}}{0.02 \cdot 400} \cong 1.2\,\mu\text{F}$$

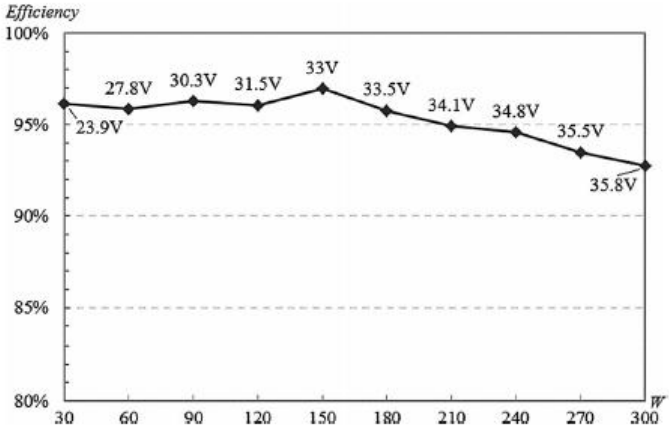

Fig. 5: Measured efficiency of the proposed SPO at various load conditions.

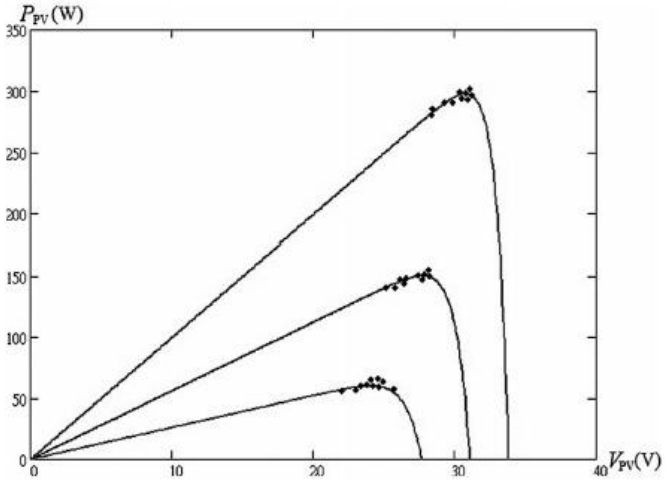

Fig. 6: MPPT accuracy distributions of the proposed SPO measured ten times.

V. EXPERIMENTAL RESULTS

Using general power supply for three test conditions, namely, low, medium, and high insolation conditions, are used to verify the various irradiation circumstances for the SPO. The low insolation condition, input voltage is 20 V and PV output power is 60 W. The measurement waveforms of the voltage and current of active switch S and diodes *D*1, *D*2 , and *D*4, as well as the voltage waveforms of capacitors *C*1, *C*2 , and *Co*, are shown in Fig. 3. For the medium insolation condition, the input voltage is 30 V and PV output load is 150 W; the measurement results are shown in Fig. 11(b). For the high insolation condition, the input voltage is 40 V and PV output power is 300 W, which is the full load condition; the measurement results are shown in Fig. 5. These current and voltage waveforms are consistent with the operating principle and the steady-state analysis. The PV simulator Agilent E4360 A is used to simulate various insolation conditions for the rest of SPO tests. The maximum SPO efficiency is 96.7%; and the full-load efficiency is about 92.8% at MPP voltage *V*mp is 35.8 V; they are shown in Fig. 5. The efficiency curve, which illustrates the maximum efficiency, is allocated at half-output power and *V*mp = 33 V of the PV module. The MPPT accuracy is defined in (44). Fig. 13 shows that the MPPT distribution of the SPO is measured ten times to verify the feasibility and capability of the MPPT control algorithm in the SPO. At an MPP of 60 W, the average accuracy is about 96.8%. At an MPP of 150 and 300 W, the average accuracy levels are 97.9% and 97.8%, respectively. The maximumMPPT accuracy is 99.9% at each irradiation condition. However, the MPPT at low MPP is less accurate than that at half and full PV output power.

VI. CONCLUSION

The high step-up SPO uses the coupled inductor with an appropriate turns ratio design and switched-capacitor technology to achieve a high-voltage gain that is 20 times higher than the input voltage. Because the leakage inductance energy of a coupled inductor is recycled and the voltage stress across the active switch S is constrained, the low *R*DS(ON) of active switch can be selected to improve maximum efficiency up to 96.7%.

As a result, full load efficiency reaches 92.8%. The highest MPPT accuracy is 99.9% and the highest average accuracy is 97.9% at *P*PV = 150 W. A 300 W SPO with a high step-up voltage gain and MPPT functions are implemented and verified.

REFERENCES

[1] Y. Fang and X. Ma, "A novel PVmicroinverter with coupled inductors and double-boost topology," IEEE Trans. Power Electron., vol. 25, no. 12, pp. 3139–3147, Dec. 2010.

[2] A. Ch. Kyritsis, E. C. Tatakis, and N. P. Papanikolaou, "Optimum design of the current-source flyback inverter for decentralized grid-connected photovoltaic systems," IEEE Trans. Energy Convers., vol. 23, no. 1,pp. 281–293, Mar. 2008.

[3] P. Tsao, "Simulation of PV systems with power optimizers and distributed power electronics," in Proc. IEEE Photovolt. Spec. Conf., Jun. 2010,pp. 389–393.

[4] D. D.-C. Lu and V. G. Agelidis, "Photovoltaic-battery-powered DC bussystem for common portable electronic devices," IEEE Trans. Power Electron., vol. 24, no. 3, pp. 849–855, Feb. 2009.

[5] L. Zhang, K. Sun,Y. Xing, L. Feng, andH.Ge, "A modular grid-connected photovoltaic generation system based on DC bus," IEEE Trans. Power Electron., vol.26, no. 2, pp. 523–531, Feb. 2011.

[6] S. M. Chen, K. R. Hu, T. J. Liang, L. S. Yang, and Y. H. Hsieh, "Implementation of high step-up solar power optimizer for DC micro grid application,"in Proc.IEEE Appl. Power Electron Conf., Feb. 2012, pp. 28–32.

[7] A. Pratt, P. Kumar, and T. V. Aldridge, "Evaluation of 400 V DC distribution in telco and data centers to improve energy efficiency," in Proc. IEEE Int. Telecommun. Energy Conf., Sep./Oct. 2007, pp. 32–39.

[8] L. Zhang, K. Sun,Y. Xing, L. Feng, andH.Ge, "A modular grid-connected photovoltaic generation system based on DC bus," IEEE Trans. PowerElectron., vol. 26, no. 2, pp. 523–531, Feb. 2011.

[9] S.M. Chen, T. J. Liang, L. S. Yang, and J. F. Chen, "A boost converter with capacitor multiplier and coupled inductor for AC module applications,"IEEE Trans.Ind. Electron., Early Access Articles, vol. PP, no. 99, p. 1.

[10] A. C. Nanakos, E. C. Tatakis, and N. P. Papanikolaou, "A weightedefficiency-oriented design methodology of flyback Inverter for AC photovoltaic modules," *IEEE Trans. Power Electron.*, vol. 27, no. 7, pp. 3221–3233, Jul. 2012.